

Intravital imaging of splenic classical monocytes modifying the hepatic CX3CR1⁺ cells motility to exacerbate liver fibrosis via spleen-liver axis

Chenlu Han¹, Yujie Zhai¹, Yuke Wang¹, Xuwen Peng¹, Xian Zhang¹, Bolei Dai¹,
Yuehong Leng¹, Zhihong Zhang^{1,2*} and Shuhong Qi^{1*}

¹Britton Chance Center and MoE Key Laboratory for Biomedical Photonics, Wuhan National Laboratory for Optoelectronics-Huazhong University of Science and Technology, Wuhan, Hubei 430074, China

²State key laboratory of digital medical engineering, School of Biomedical Engineering, Hainan University, Haikou, Hainan 570228, China

* Correspondence: Zhihong Zhang, czyzzh@mail.hust.edu.cn;
Shuhong Qi, qishuhong@hust.edu.cn;

Address: Room G304, Britton Chance Center for Biomedical Photonics, Wuhan National Laboratory for Optoelectronics-Huazhong University of Science and Technology, Wuhan, Hubei 430074, China

Fax: +86-27-87792034; Tel: +86-27-87792033;

Zhihong Zhang (czyzzh@mail.hust.edu.cn) and Shuhong Qi (qishuhong@hust.edu.cn) are the corresponding authors for communication with the Editorial and Production offices.

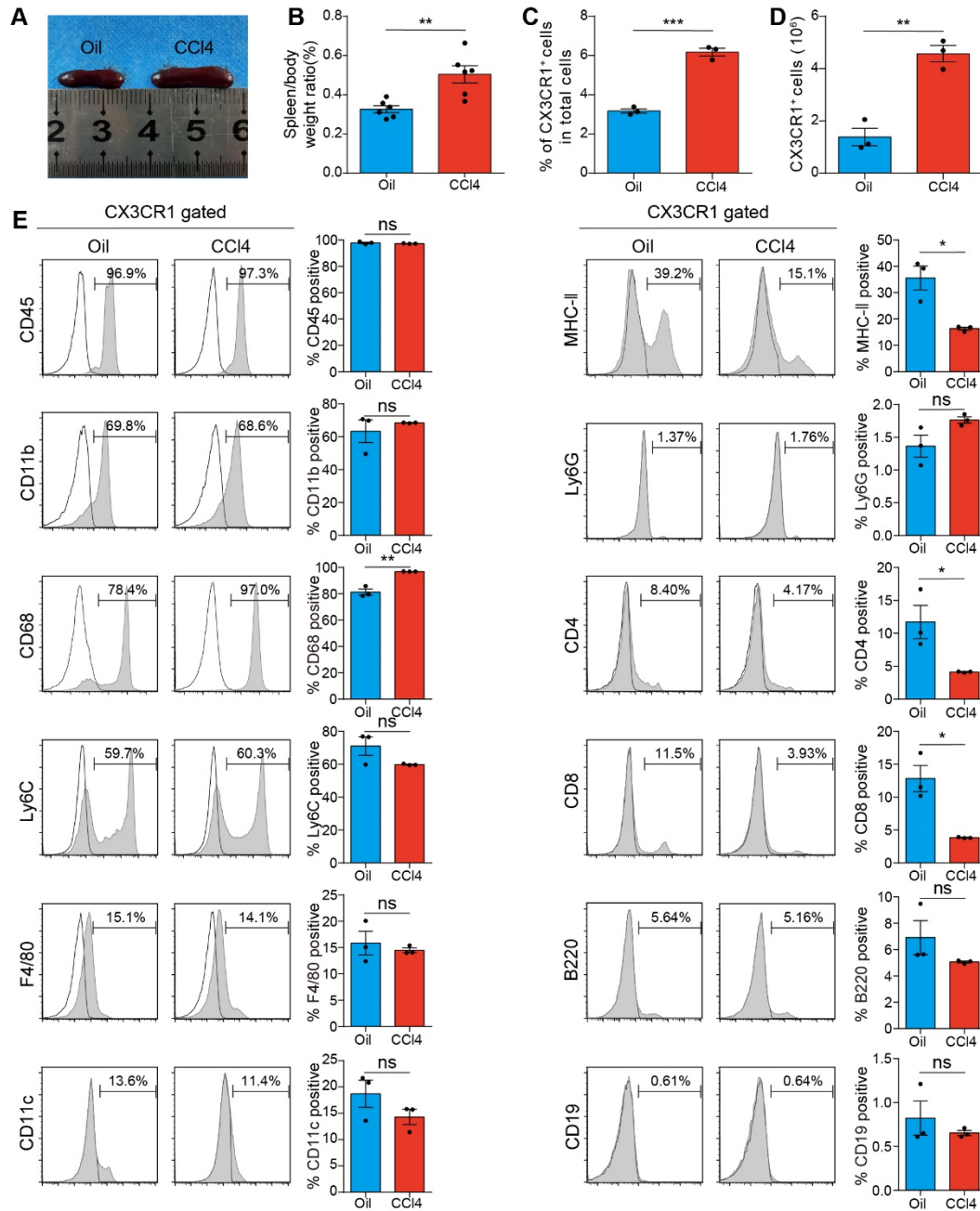


Figure S1. Flow cytometry analysis of splenic CX3CR1⁺ cells and their phenotypic characteristics in Oil/CCl4-treated mice. (A) Spleen in the Oil and CCl4-treated mice. (B) Spleen/body weight ratio was calculated (n = 6 mice per group). (C) The percentage of splenic CX3CR1⁺ cells in Oil-treated mice or CCl4-treated mice (n = 3 mice per group). (D) The number of splenic CX3CR1⁺ cells in Oil-treated mice or CCl4-treated mice (n = 3 mice per group). (E) The phenotypic characteristics of splenic CX3CR1⁺ cells in Oil-treated mice or CCl4-treated mice (n = 3 mice per group). Data are presented as the mean \pm SEM.

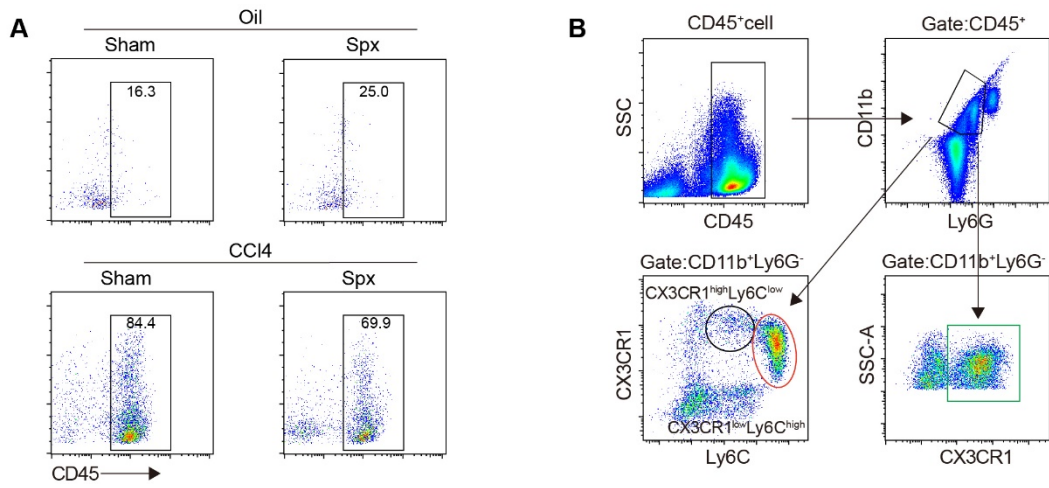


Figure S2. Flow cytometry analysis of hepatic CX3CR1⁺ cells and their subsets in Oil/CCI4-treated mice with or without splenectomy. (A) Gating strategy of hepatic CD45⁺ cells. (B) Gating strategy of hepatic CX3CR1⁺ cells and their subsets.

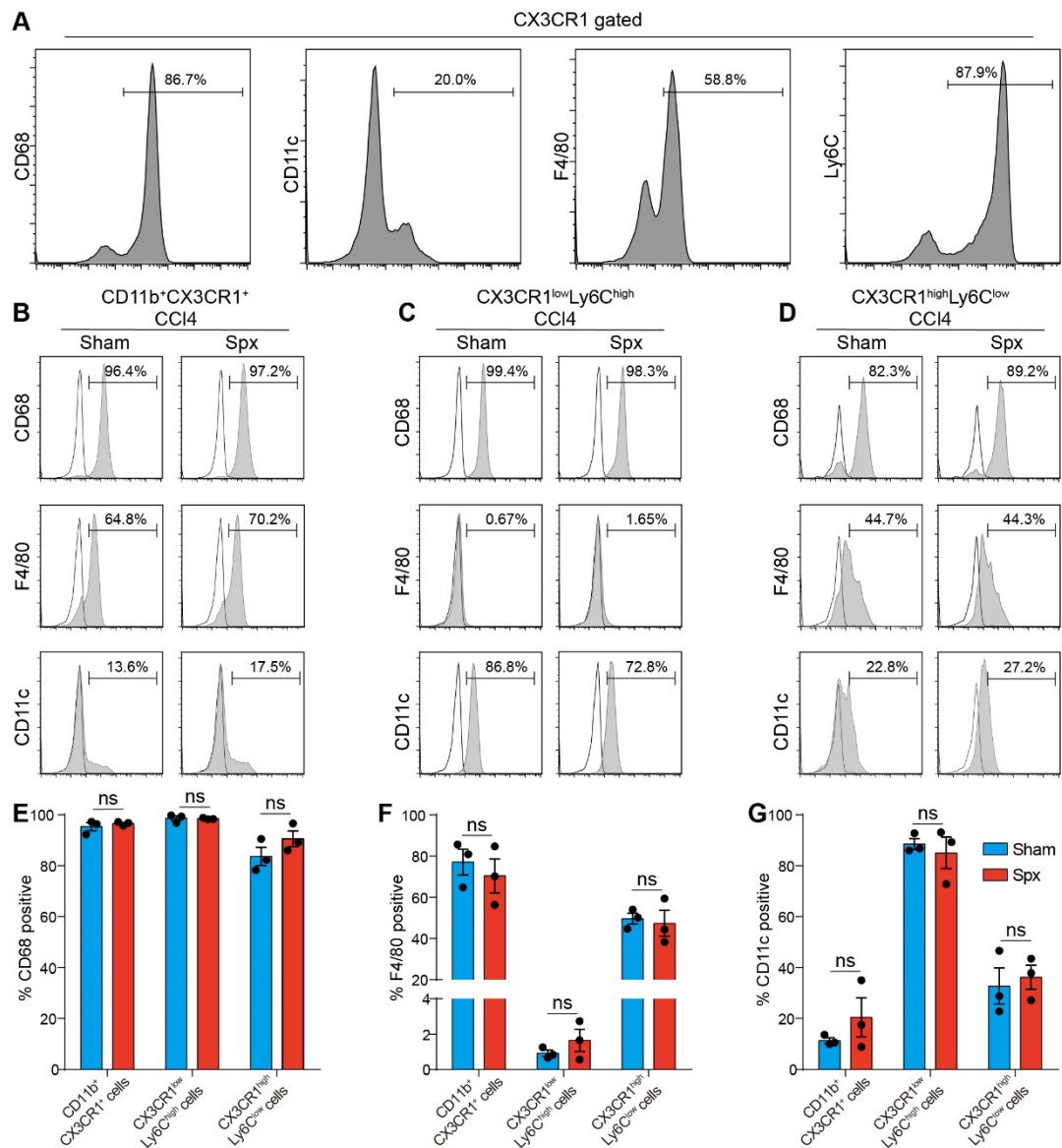


Figure S3. Phenotypic characteristics of CX3CR1⁺ cells and their subsets in the livers of CCl4-treated mice with or without splenectomy. (A) Phenotypic analysis of hepatic CX3CR1⁺ cells from CCl4-treated mice by flow cytometry. (B-D) The hepatic CX3CR1⁺ cells and their subsets have distinct phenotypic profiles. (E-G) Phenotypic analysis of hepatic CD11b⁺CX3CR1⁺ cells and their subsets from fibrotic mice at one week after splenectomy by flow cytometry (n = 3 mice per group). Data are presented as the mean ± SEM.

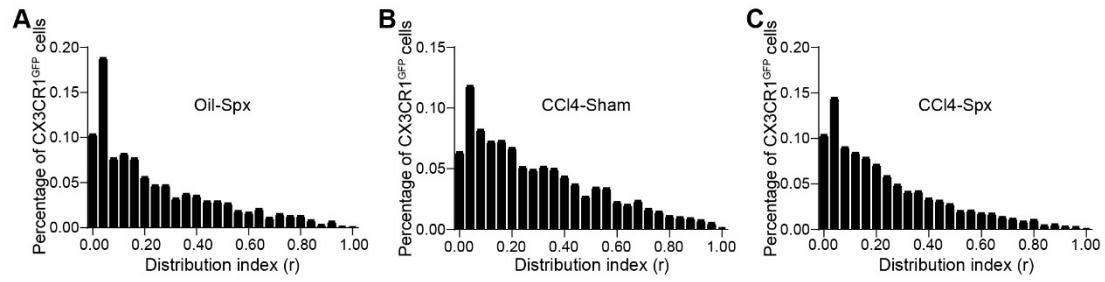


Figure S4. The distribution of CX3CR1^{GFP} cells in each distribution index (r) from different groups. (A) The distribution of CX3CR1^{GFP} cells in each distribution index (r) from Oil-treated group with Spx; the bin value is 0.04. **(B)** The distribution of CX3CR1^{GFP} cells in each distribution index (r) from CCl4-treated group with Sham; the bin value is 0.04. **(C)** The distribution of CX3CR1^{GFP} cells in each distribution index (r) from CCl4-treated group with Spx; the bin value is 0.04.

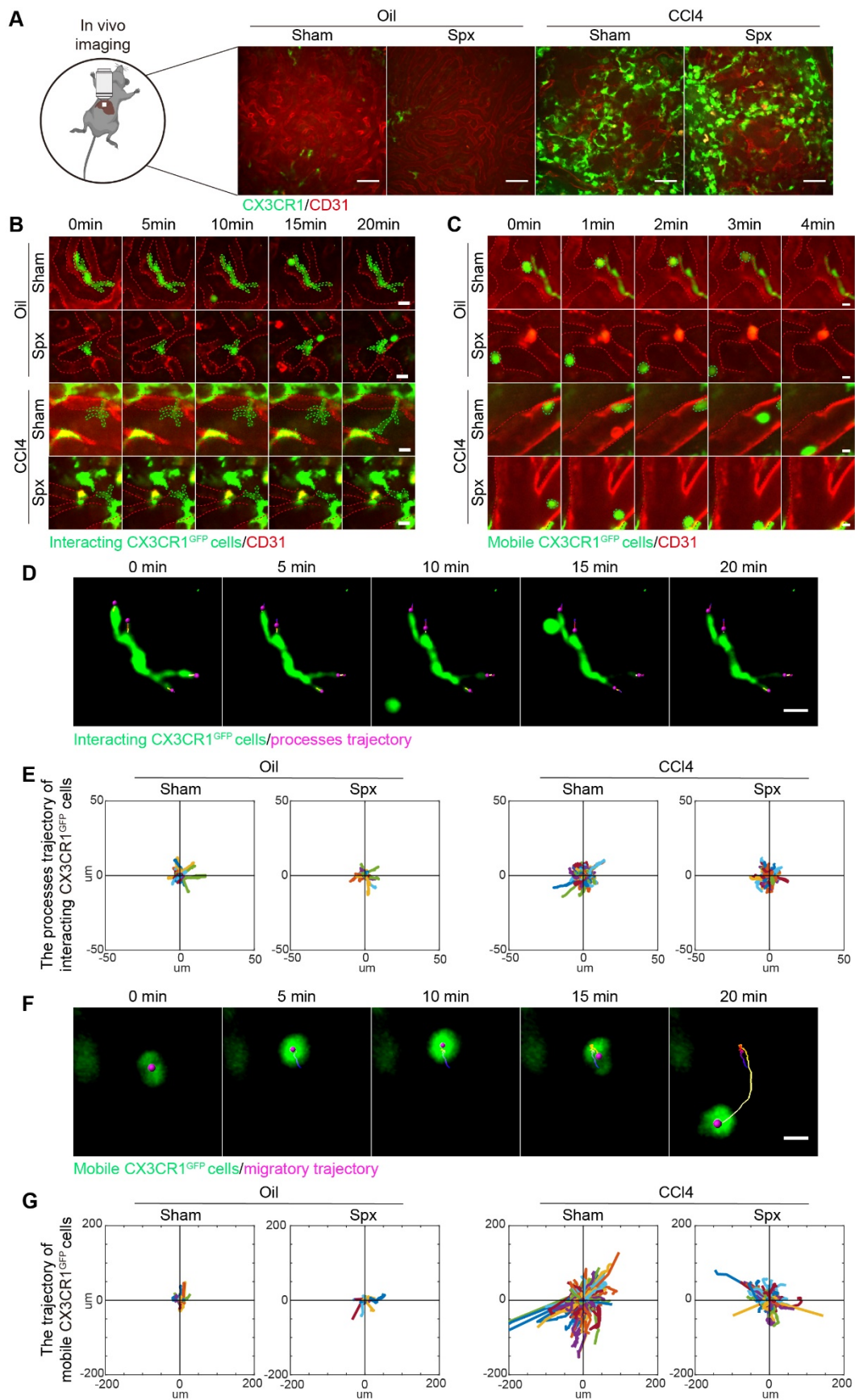


Figure S5. Intravital imaging of hepatic CX3CR1^{GFP} cell subtypes in the Oil/CCl4-treated mice with or without splenectomy. (A) Representative fluorescence images of CX3CR1^{GFP} cells

in the liver of Oil/CCl₄-treated mice with or without splenectomy. Green: CX3CR1^{GFP} cells; Red: AF647 anti-CD31 labeled hepatic vessels. Scale bar, 50 μm. **(B)** The interacting CX3CR1^{GFP} cells with motile processes cause distinct shape changes during 20 minutes. Green: CX3CR1^{GFP} cells; Red: AF647 anti-CD31 labeled hepatic vessels. Scale bar, 10 μm. **(C)** The rapid movement of mobile CX3CR1^{GFP} cells in the hepatic vessels. Green: CX3CR1^{GFP} cells; Red: AF647 anti-CD31 labeled hepatic vessels. Scale bar, 2 μm. **(D)** Representative images showing the processes trajectory of interacting CX3CR1^{GFP} cell over a 20-minute period. Scale bar, 10 μm. **(E)** The processes trajectory of interacting CX3CR1^{GFP} cells in the liver parenchyma. **(F)** Representative images showing the migratory trajectory of mobile CX3CR1^{GFP} cell over a 20-minute period. Scale bar, 5 μm. **(G)** The trajectory of mobile CX3CR1^{GFP} cells in the hepatic vessels.

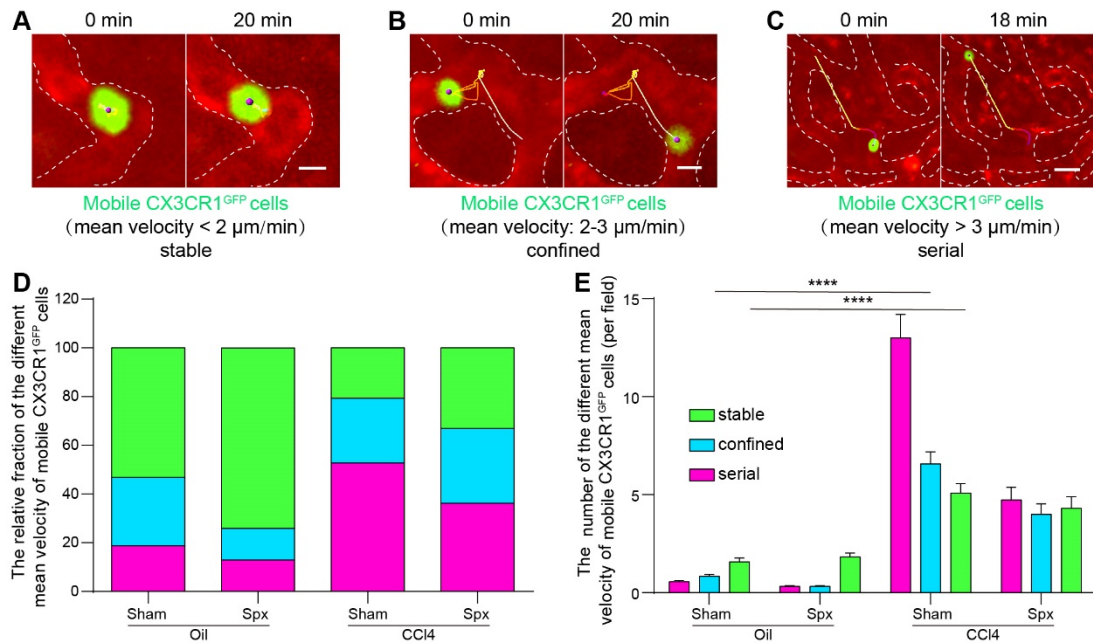


Figure S6. The different mobile type of hepatic CX3CR1^{GFP} cell in the Oil/CCl4-treated mice with or without splenectomy. (A) Representative images showing the migratory trajectory of mobile CX3CR1^{GFP} cell with mean velocity less than 2 μm/min (“stable” type) over a 20-minute period. Green: CX3CR1^{GFP} cells; Red: AF647 anti-CD31 labeled hepatic vessels. White dotted line shows the vessels. Scale bar, 5 μm. (B) Representative images showing the migratory trajectory of mobile CX3CR1^{GFP} cell with mean velocity between 2-3 μm/min (“confined” type) over a 20-minute period. Green: CX3CR1^{GFP} cells; Red: AF647 anti-CD31 labeled hepatic vessels. White dotted line shows the vessels. Scale bar, 5 μm. (C) Representative images showing the migratory trajectory of mobile CX3CR1^{GFP} cell with mean velocity more than 3 μm/min (“serial” type) over a 20-minute period. Green: CX3CR1^{GFP} cells; Red: AF647 anti-CD31 labeled hepatic vessels. White dotted line shows the vessels. Scale bar, 15 μm. (D) The relative fraction of the different mobile type of CX3CR1^{GFP} cells in the liver of Oil/CCl4-treated mice with or without splenectomy (n = 22-28 fields, from 3 mice per group). (E) The number of the different mobile type of CX3CR1^{GFP} (per field) in the liver of Oil/CCl4-treated mice with or without splenectomy (n = 22-28 fields, from 3 mice per group).

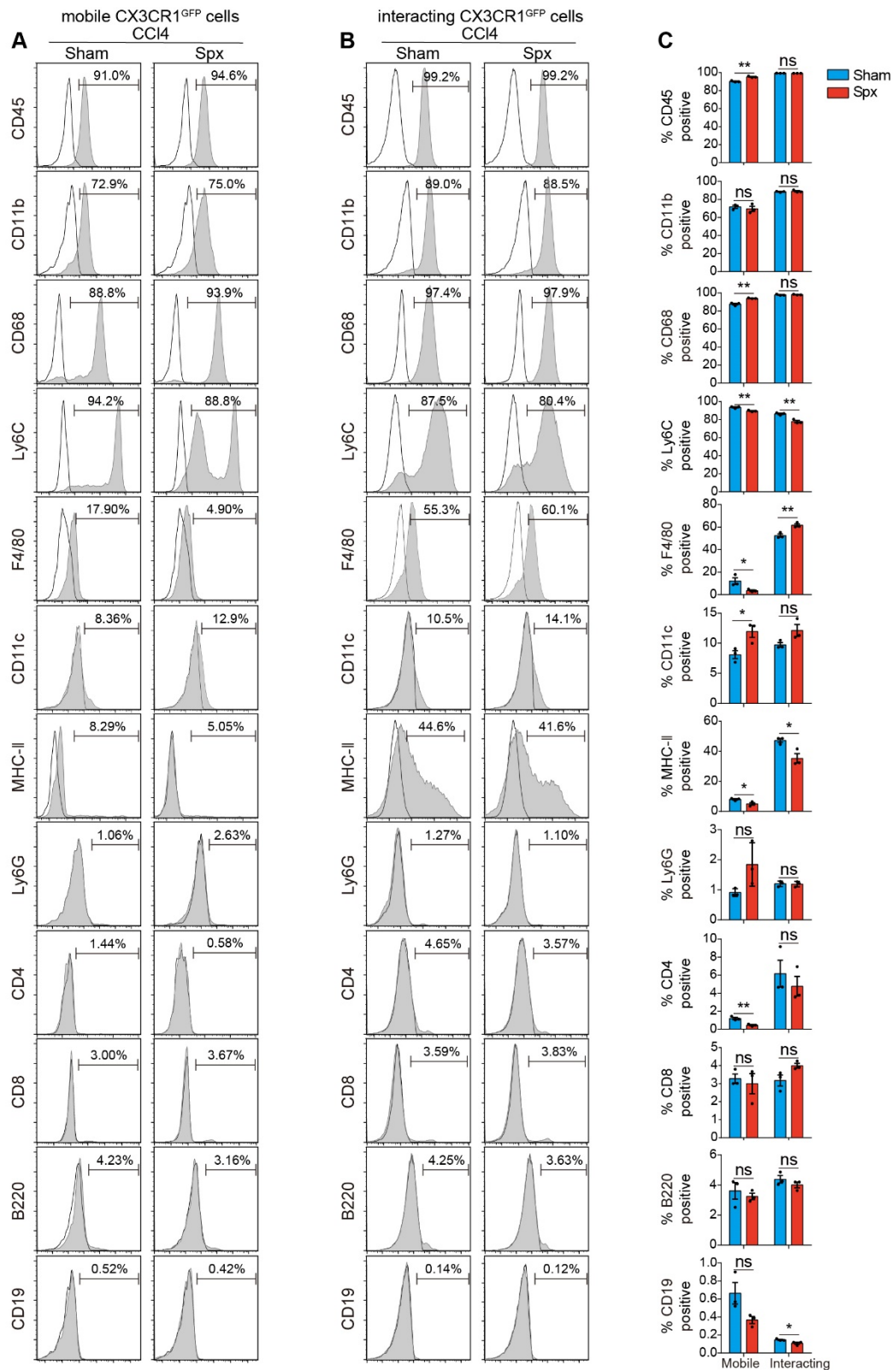


Figure S7. Phenotypic characteristics of mobile CX3CR1^{GFP} cells and interacting CX3CR1^{GFP} cells in the livers of CCI4-treated mice with or without splenectomy. (A-B) The surface marker profile of hepatic mobile CX3CR1^{GFP} cells and interacting CX3CR1^{GFP} cells. **(C)** Phenotypic analysis of hepatic mobile CX3CR1^{GFP} cells and interacting CX3CR1^{GFP} cells from fibrotic mice at

24 h after splenectomy by flow cytometry (n = 3 mice per group). Data are presented as the mean \pm SEM.

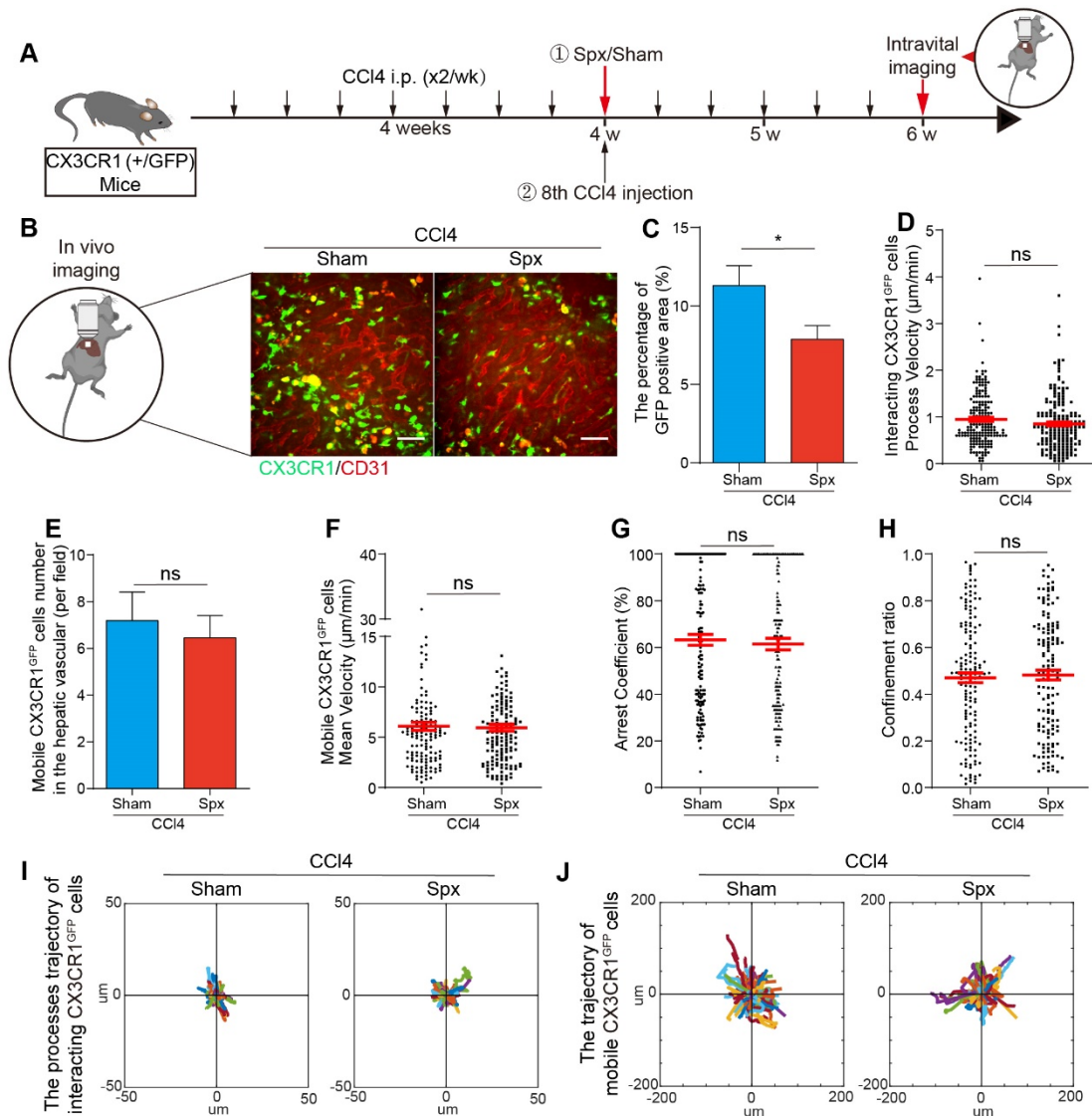


Figure S8. Intravital imaging of CX3CR1^{GFP} cells in the livers of CCl4-treated mice with or without splenectomy at 14 days after splenectomy. (A) Schedules of generation of liver fibrosis model, the splenectomy and intravital imaging. (B) Representative fluorescence images of the CX3CR1^{GFP} cells in the livers of CCl4-treated mice with or without splenectomy. Green: CX3CR1^{GFP} cells; Red: AF647 anti-CD31 labeled hepatic vessels. Scale bar, 50 μ m. (C) The positive areas of GFP were quantified using Image J software (from 3 mice per group). (D) The velocity of interacting CX3CR1^{GFP} cells processes in the liver parenchyma. Each dot represents a single cell process, and the red bars indicate mean values (3 mice per group). (E) The cell number of mobile CX3CR1^{GFP} cells in the hepatic vessels of CCl4-treated mice with or without splenectomy (n = 21-22 fields, from 3 mice per group). (F-H) Scatter plots of mean velocity (F), arrest coefficient (G), and confinement ratio (H) of mobile CX3CR1^{GFP} cells in the hepatic vessels of CCl4-treated mice with or without splenectomy (n = 21-22 fields, from 3 mice per group). Each dot represents a

single cell, and the red bars indicate mean values. Data are presented as mean \pm SEM. **(I)** The processes trajectory of interacting CX3CR1^{GFP} cells in the liver parenchyma. **(J)** The trajectory of mobile CX3CR1^{GFP} cells in the hepatic vessels.

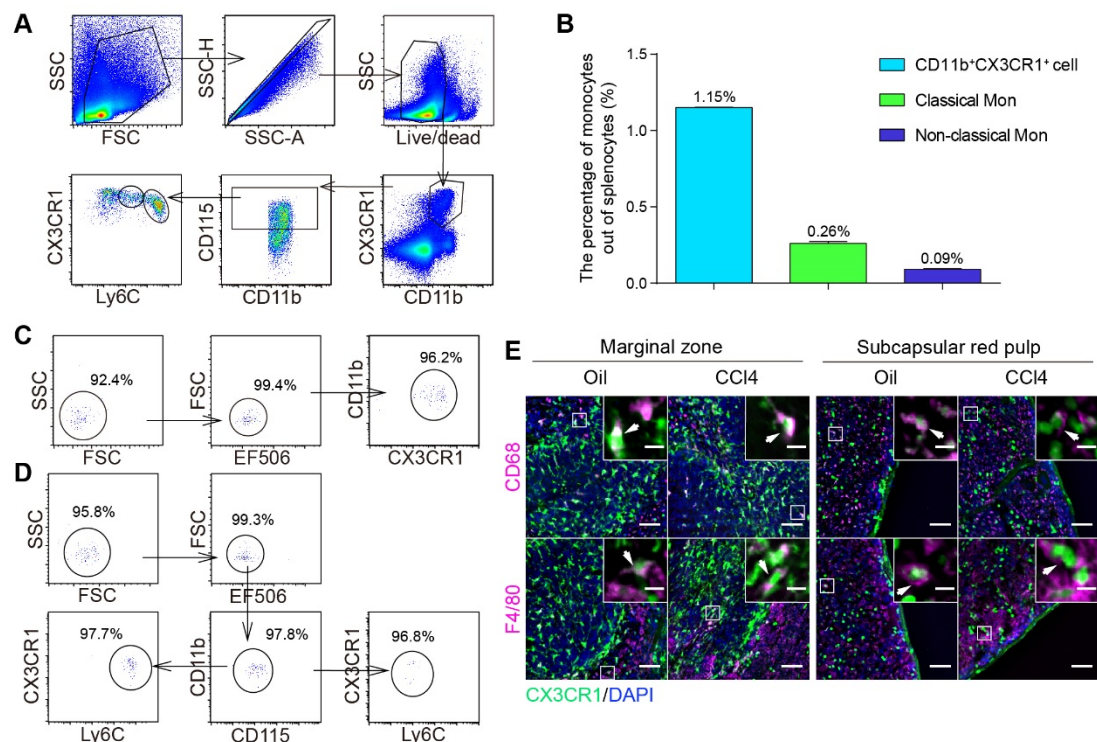


Figure S9. Flow cytometry analysis and immunofluorescence staining to identify splenic CX3CR1⁺ cells and their subsets in the spleen of Oil/CCl₄-treated mice. (A) Gating strategy of splenic classical monocytes and non-classical monocytes. **(B)** The percentage of CD11b⁺ CX3CR1⁺ cells, classical monocytes and non-classical monocytes out of splenocytes in the fibrotic spleen (n = 3 mice per group). **(C-D)** The percentage of sorted splenic CD11b⁺ CX3CR1⁺ cells **(C)**, CD11b⁺ CD115⁺ CX3CR1^{low} Ly6C^{high} cells and CD11b⁺ CD115⁺ CX3CR1^{high} Ly6C^{low} cells **(D)**. **(E)** The cell surface receptor profile of CX3CR1^{GFP} cells in the marginal zone and subcapsular red pulp of the fibrotic spleen was examined by immunofluorescence staining. Green: CX3CR1^{GFP} cells; Blue: DAPI; Magenta: CD68/ F4/80. Scale bar (large image), 50 μm. Scale bar (small image), 10 μm. White arrows indicate CX3CR1^{GFP} cells.

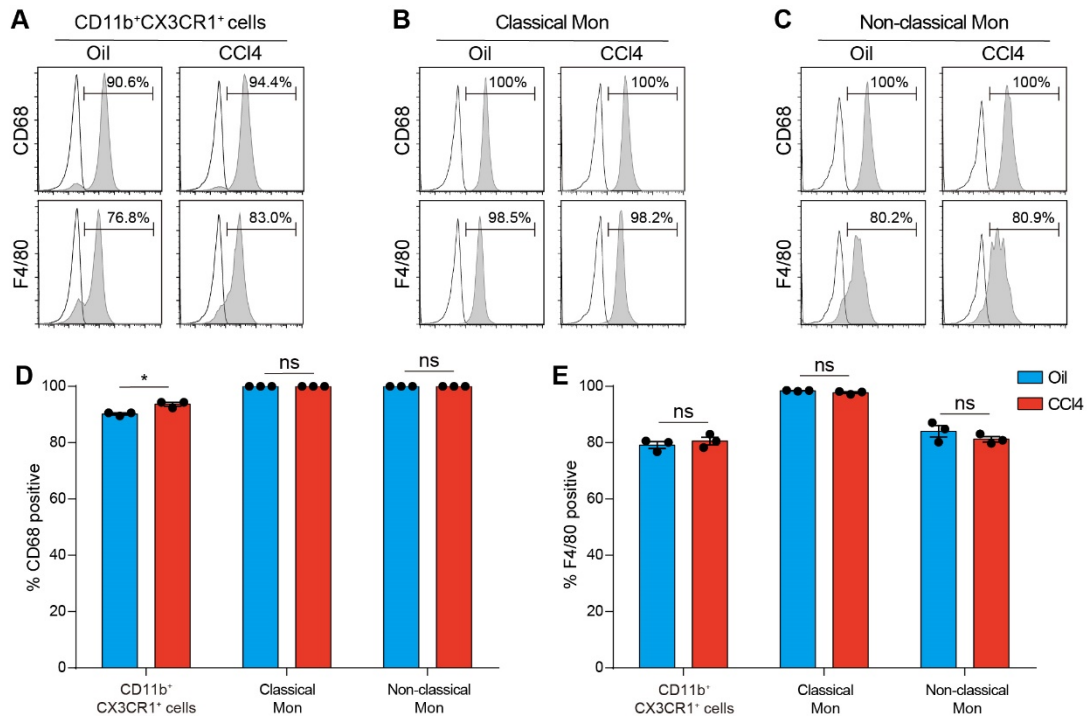


Figure S10. Phenotypic characteristics of splenic CX3CR1⁺ cells and their subsets from Oil/CCl4-treated mice by flow cytometry. (A-C) The splenic CX3CR1⁺ cells and their subsets have distinct phenotypic profiles. (D-E) Phenotypic analysis of CD11b⁺ CX3CR1⁺ cells and their subsets in the spleen of Oil and CCl4-treated mice by flow cytometry (n = 3 mice per group). Data are presented as the mean ± SEM.

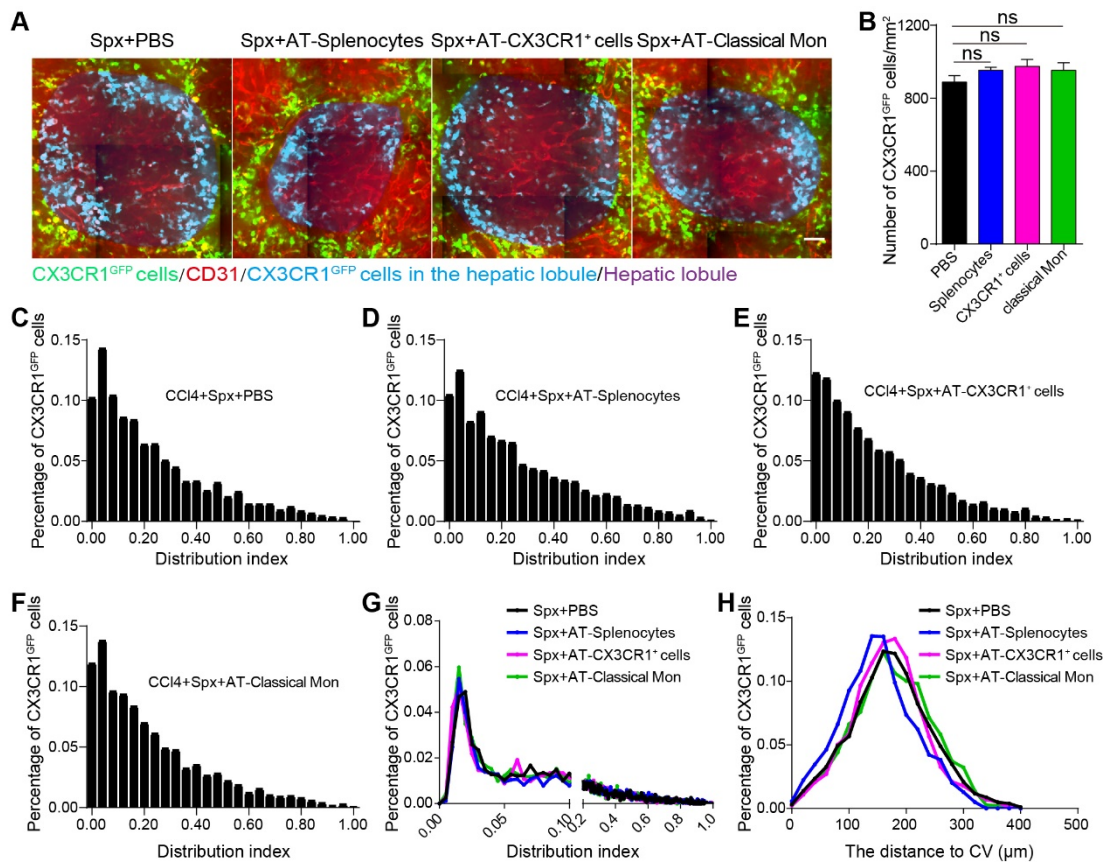


Figure S11. Intravital imaging of the spatial distribution of CX3CR1^{GFP} cells in the fibrotic liver after adoptively transferring splenic cells. (A) Intravital imaging of CX3CR1^{GFP} cells distribution in the hepatic lobule. Green: CX3CR1^{GFP} cells; Red: AF647 anti-CD31 labeled hepatic vessels; Blue: CX3CR1^{GFP} cells in the hepatic lobule; Magenta: Hepatic lobule. Scale bar, 50 μ m. (B) The density of CX3CR1^{GFP} cells in one hepatic lobule (n = 10-21, from 3 mice per group). Data are presented as mean \pm SEM. (C-F) The distribution of CX3CR1^{GFP} cells in each distribution index from different groups; the bin value is 0.04. (G) The distribution curves of CX3CR1^{GFP} cells in each distribution index from different groups; the bin value is 0.005. (H) The distance of CX3CR1^{GFP} cells to the hepatic central vein (CV) in the hepatic lobules.

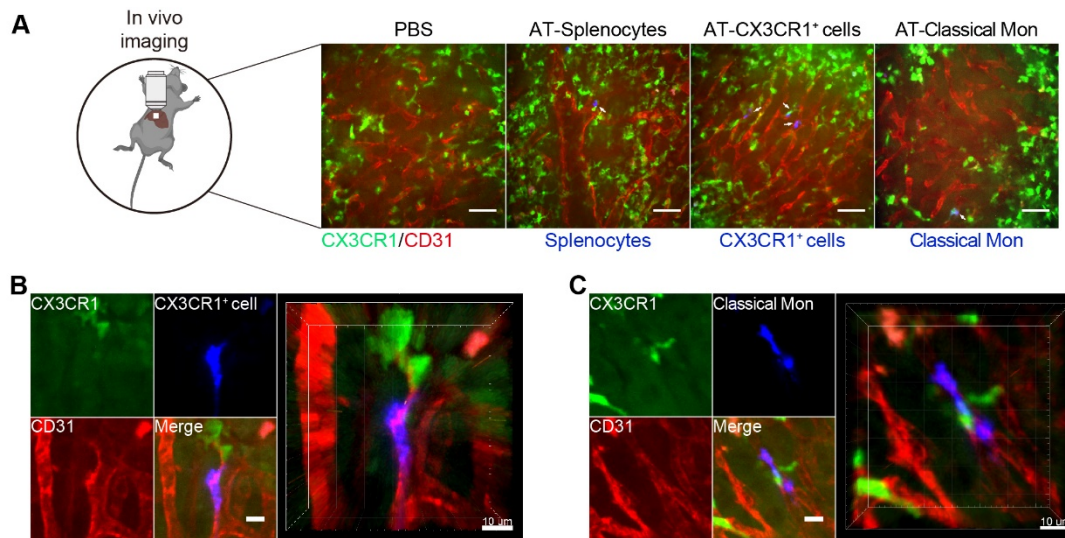


Figure S12. Imaging of the migration behavior of endogenous $\text{CX3CR1}^{\text{GFP}}$ cells and adoptive splenic cells in the fibrotic liver. (A) Intravital imaging of adoptive splenic cells in the liver. Green: $\text{CX3CR1}^{\text{GFP}}$ cells; Red: AF647 anti-CD31 labeled hepatic vessels; Blue: Splenocytes. Scale bar, 50 μm . White arrows indicate the adoptive splenic cells. **(B)** Immunofluorescence imaging of adoptive splenic CX3CR1^+ cells in the liver. Green: $\text{CX3CR1}^{\text{GFP}}$ cells; Red: AF647 anti-CD31 labeled hepatic vessels; Blue: Splenic CX3CR1^+ cells. Scale bar, 10 μm . **(C)** Immunofluorescence imaging of adoptive splenic classical monocytes in the liver. Green: $\text{CX3CR1}^{\text{GFP}}$ cells; Red: AF647 anti-CD31 labeled hepatic vessels; Blue: Splenic classical monocytes. Scale bar, 10 μm .

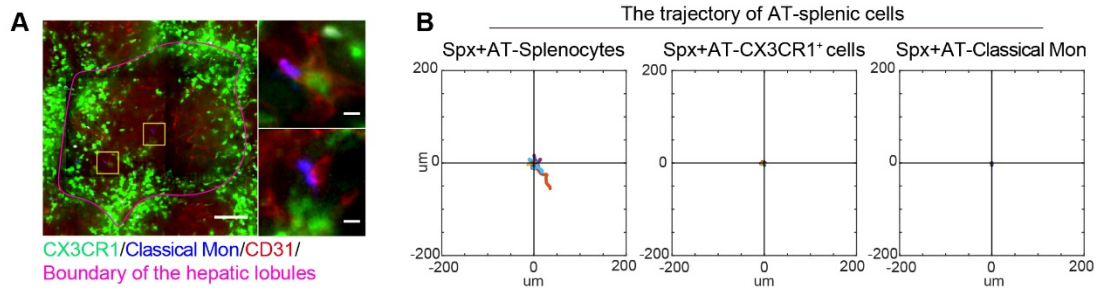


Figure S13. Intravital imaging revealed the localization and migration behavior of adoptive splenic cells in the fibrotic liver after adoptively transferring splenic cells. (A) The distribution of adoptive splenic classical monocytes in the hepatic lobules. Green: CX3CR1^{GFP} cells; Blue: Classical monocytes; Red: AF647 anti-CD31 labeled hepatic vessels; Magenta: Boundary of the hepatic lobules. Scale bar, 100 μm . High-magnification views of the adoptive splenic classical monocytes in the liver are shown on the right. Scale bar, 10 μm . **(B)** The trajectory of adoptive splenic cells in different groups.

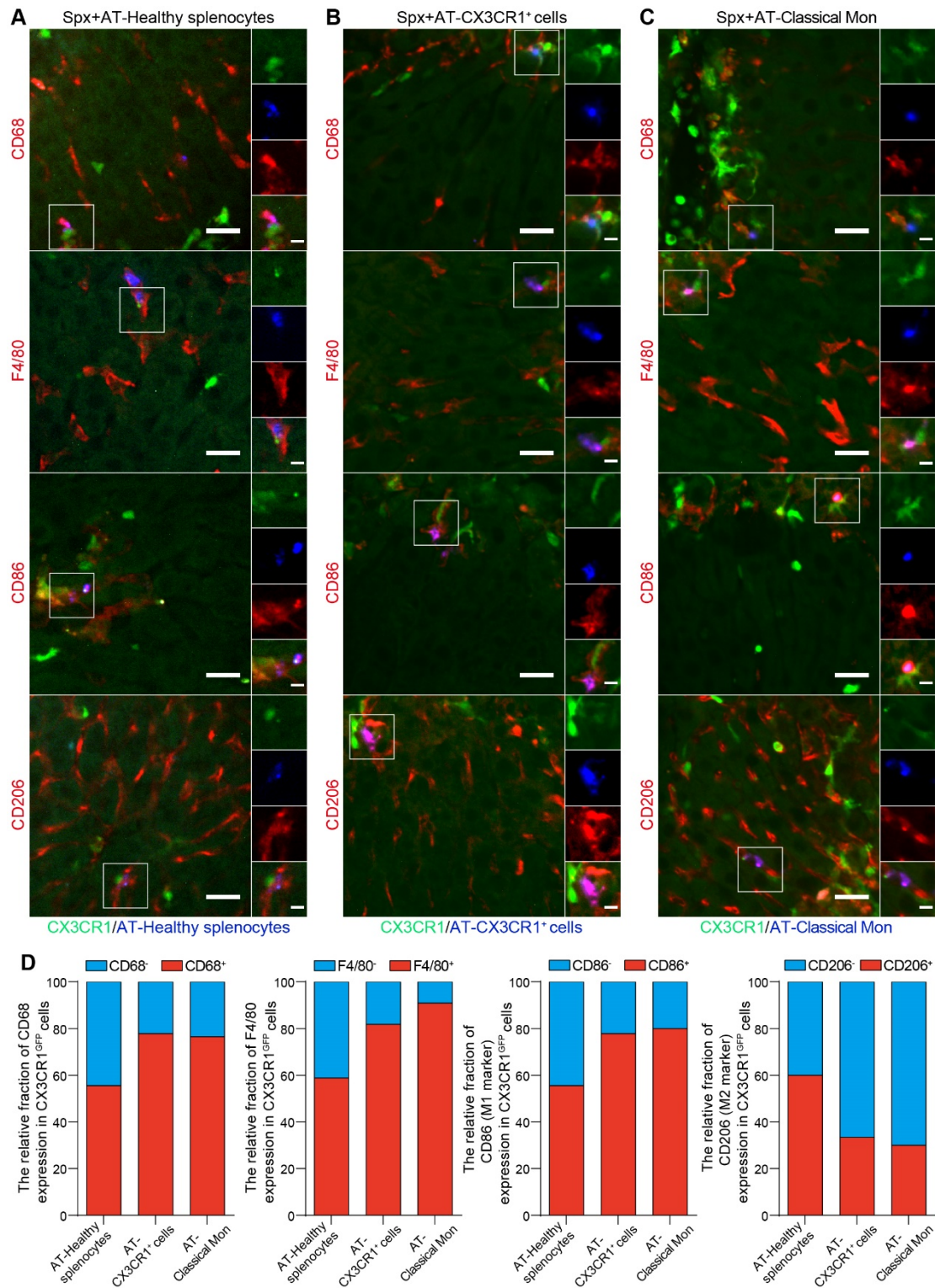


Figure S14. The phenotypic characteristics of neighboring endogenous CX3CR1^{GFP} cells contacted with adoptive splenic cells in the fibrotic liver. (A) Phenotypic characteristics of neighboring endogenous CX3CR1^{GFP} cells contacted with adoptive splenocytes from healthy mice. Scale bar (large image), 25 μ m. Scale bar (small image), 8 μ m. **(B)** Phenotypic characteristics of neighboring endogenous CX3CR1^{GFP} cells contacted with adoptive splenic CX3CR1⁺ cells from

fibrotic mice. Scale bar (large image), 25 μm . Scale bar (small image), 8 μm . (C) Phenotypic characteristics of neighboring endogenous CX3CR1^{GFP} cells contacted with adoptive splenic classical monocytes from fibrotic mice. Scale bar (large image), 25 μm . Scale bar (small image), 8 μm . (D) Phenotypic analysis of neighboring endogenous CX3CR1^{GFP} cells contacted with adoptive splenic cells (The proportion of CD68 expression in neighboring endogenous CX3CR1^{GFP} cells: n = 9-18 cells, from 3 mice per group; The proportion of F4/80 expression in neighboring endogenous CX3CR1^{GFP} cells: n = 17-33 cells, from 3 mice per group; The proportion of CD86 expression in neighboring endogenous CX3CR1^{GFP} cells: n = 9-10 cells, from 3 mice per group; The proportion of CD206 expression in neighboring endogenous CX3CR1^{GFP} cells: n = 9-10 cells, from 3 mice per group).

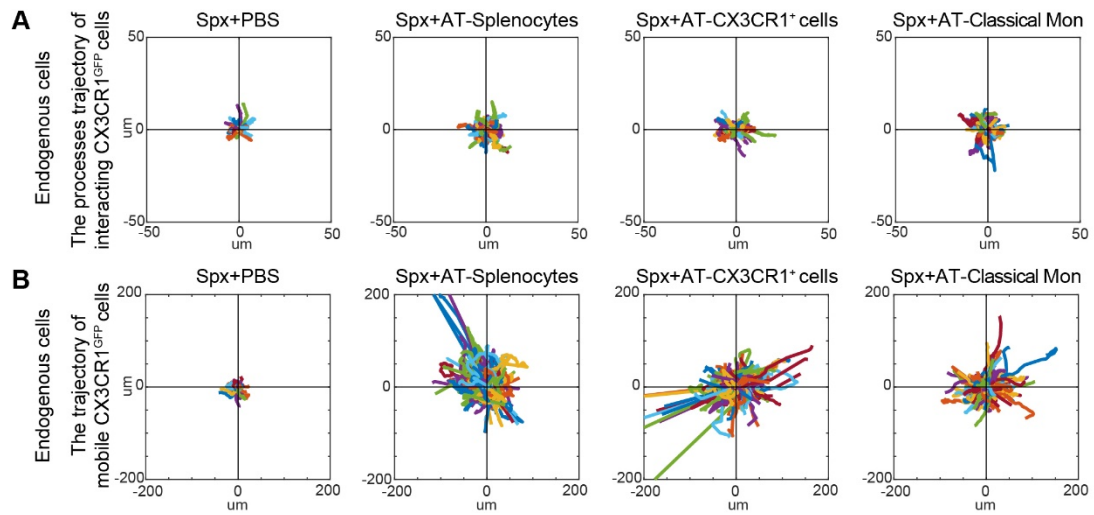


Figure S15. Intravital imaging revealed the migration behavior of hepatic endogenous CX3CR1^{GFP} cells in the fibrotic liver after adoptively transferring splenic cells. (A) The processes trajectory of interacting CX3CR1^{GFP} cells in the liver parenchyma. (B) The trajectory of mobile CX3CR1^{GFP} cells in the hepatic vessels.

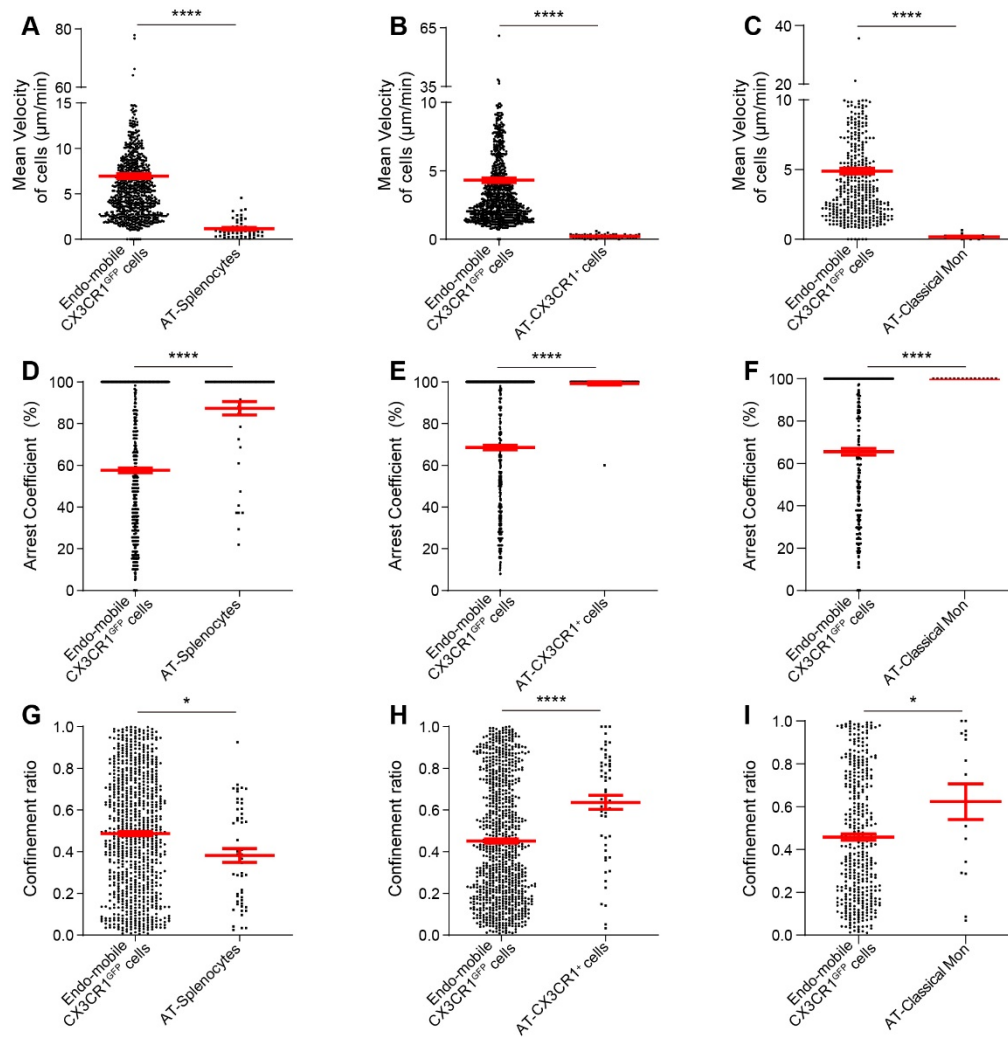


Figure S16. Intravital imaging revealed the migration characteristics of hepatic endogenous CX3CR1^{GFP} cells and adoptive splenic cells. (A-C) Scatter plots of mean velocity of endo-mobile CX3CR1^{GFP} cells and adoptive splenic cells in different groups (3 mice per group). (D-F) Scatter plots of arrest coefficient of endo-mobile CX3CR1^{GFP} cells and adoptive splenic cells in different groups (3 mice per group). (G-I) Scatter plots of confinement ratio of endo-mobile CX3CR1^{GFP} cells and adoptive splenic cells in different groups (3 mice per group).

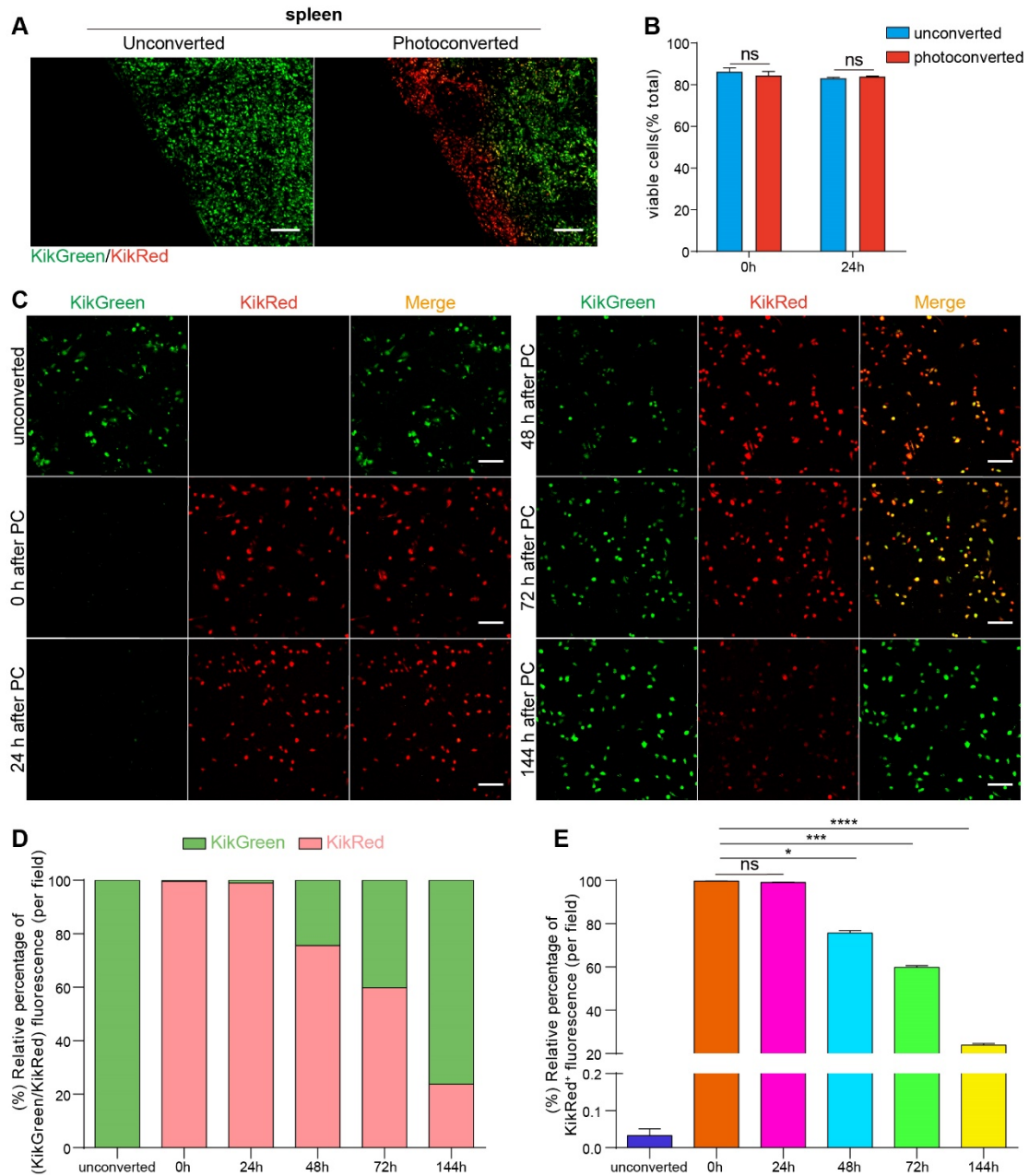


Figure S17. The effect of the procedure of CX3CR1-KikGR photoconversion on cell viability and the stability of KikRed protein levels in CX3CR1⁺ cells. (A) Immunofluorescence imaging of unconverted and photoconverted spleen. Scale bar, 100 μm . (B) The viability of splenocytes from unconverted and photoconverted CX3CR1-KikGR transgenic mice was assessed using the fixable viability dye eFluor506 and analyzed by flow cytometry immediately (0 h) or 24 h after photoconversion (n = 3 mice per group). (C) Mouse peritoneal macrophages isolated from unconverted CX3CR1-KikGR transgenic mice were photoconverted by exposure to the 405 nm light (cells was exposed for 3 minutes, 200 mW/cm^2) *in vitro* and analyzed by confocal imaging immediately (0 h) or after culture for 24h, 48h, 72h and 144 h at 37 $^{\circ}\text{C}$. Scale bar, 50 μm . (D) The

relative percentage of (KikGreen/KikRed) fluorescence of CX3CR1⁺ mouse peritoneal macrophage was detected by confocal imaging. (n = 9 fields). (E) The relative percentage of KikRed⁺ fluorescence of CX3CR1⁺ mouse peritoneal macrophage was detected by confocal imaging. (n = 9 fields).

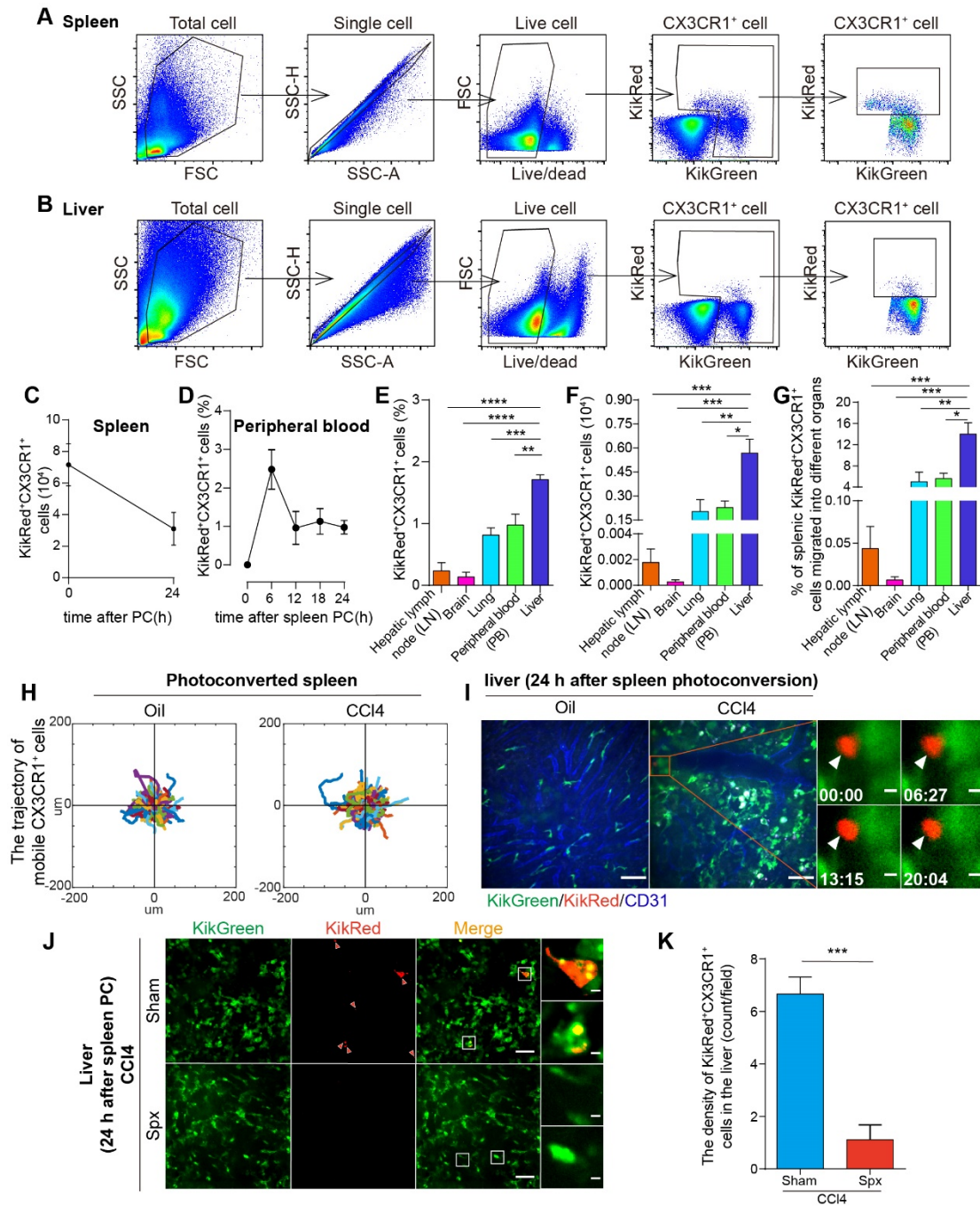


Figure S18. Distinct dynamics of CX3CR1⁺ KikRed⁺ cells in the photoconverted spleen and liver from the Oil and CCl₄-treated mice. (A) Gating strategy of splenic CX3CR1⁺ KikRed⁺ cells. **(B)** Gating strategy of hepatic CX3CR1⁺ KikRed⁺ cells. **(C)** The number of photoconverted splenic CX3CR1⁺ KikRed⁺ cells egressed from the spleen (n = 4 mice per group). **(D)** The percentage of the CX3CR1⁺ KikRed⁺ cells among CX3CR1⁺ cells in the peripheral blood over a 24-hour period (n = 3 mice per group). **(E)** The percentage of CX3CR1⁺ KikRed⁺ cells among CX3CR1⁺ cells in different organs (lymph node, brain, lung, peripheral blood and liver) at 24 h after photoconversion (n = 3-5 mice per group). **(F)** The number of splenic CX3CR1⁺ KikRed⁺ cells in different organs

(lymph node, brain, lung, peripheral blood and liver) at 24 h after photoconversion (n = 3-5 mice per group). **(G)** The percentage of splenic CX3CR1⁺ KikRed⁺ cells migrated into different organs (lymph node, brain, lung, peripheral blood and liver) at 24 h after photoconversion (n = 3-5 mice per group). **(H)** The trajectory of mobile splenic CX3CR1⁺ cells in the Oil and CCl₄-treated mice. **(I)** Intravital imaging of the liver of Oil and CCl₄-treated mice 24 h after spleen-specific photoconversion. Green: KikGreen; Red: KikRed; Blue: AF647 anti-CD31 labeled hepatic vessels. Scale bar, 50 μm. High-magnification views of splenic CX3CR1⁺ KikRed⁺ cells in the fibrotic liver are shown on the right. Scale bar, 5 μm. White arrows indicate splenic CX3CR1⁺ KikRed⁺ cells. **(J)** Intravital imaging of splenic CX3CR1⁺ KikRed⁺ cells in fibrotic livers of mice that received spleen-specific photoconversion at 24 h after splenectomy. Green: KikGreen; Red: KikRed. Scale bar, 50 μm. High-magnification views of splenic CX3CR1⁺ KikRed⁺ cells in the fibrotic liver are shown on the right. Scale bar, 5 μm. Red arrows indicate KikRed⁺ cells. **(K)** The splenic CX3CR1⁺ KikRed⁺ cells in livers were counted (cells/field). (n = 9 fields, from 3 mice per group).

Movie S1 and S2: Intravital imaging of CX3CR1^{GFP} cells in the livers of Oil/CCl4-treated mice at 24h after splenectomy. The time-lapse intravital imaging was acquired by a 20×/0.75 NA objective.

CX3CR1^{GFP} cells are shown in green, and the AF647 anti-CD31 labeled hepatic vessels are shown in red.

Scale bar, 50 μm.

Movie S3: Intravital imaging of CX3CR1^{GFP} cells in the livers of CCl4-treated mice at 14d after splenectomy. The time-lapse intravital imaging was acquired by a 20×/0.75 NA objective. CX3CR1^{GFP}

cells are shown in green, and the AF647 anti-CD31 labeled hepatic vessels are shown in red. Scale bar, 50 μm.

μm.

Movie S4 and S5: Intravital imaging of hepatic CX3CR1^{GFP} cells and adoptive splenic cells in the CCl4-treated mice with splenectomy at 24h after adoptive transferring of splenic cells. The time-lapse intravital imaging was acquired by a 20×/0.75 NA objective. CX3CR1^{GFP} cells are shown in green,

adoptive splenic cells are shown in blue and the AF647 anti-CD31 labeled hepatic vessels are shown in red. Scale bar, 50 μm.

red. Scale bar, 50 μm.

Movie S6: Immunofluorescence imaging of hepatic CX3CR1^{GFP} cells and splenic CX3CR1⁺ cells in the CCl4-treated mice with splenectomy at 24h after adoptive transferring of splenic cells.

The immunofluorescence imaging was acquired by a 20×/0.75 NA objective. CX3CR1^{GFP} cells are shown in green, splenic CX3CR1⁺ cells are shown in blue and the AF647 anti-CD31 labeled hepatic vessels are shown in red. Scale bar, 10 μm.

Movie S7: Immunofluorescence imaging of hepatic CX3CR1^{GFP} cells and splenic classical monocytes in the CCl4-treated mice with splenectomy at 24h after adoptive transferring of splenic cells. The immunofluorescence imaging was acquired by a 20×/0.75 NA objective. CX3CR1^{GFP}

cells are shown in green, splenic classical monocytes are shown in blue and the AF647 anti-CD31 labeled hepatic vessels are shown in red. Scale bar, 10 μm.

Movie S8: Intravital imaging of splenic CX3CR1⁺ cells in Oil/CCl4-treated mice after spleen photoconversion. The time-lapse intravital imaging was acquired by a 20×/0.75 NA objective.

CX3CR1⁺ cells are shown in green, photoconverted CX3CR1⁺ cells are shown in red and the AF647 anti-CD31 labeled splenic vessels are shown in blue. Scale bar, 50 μm.

Movie S9: Intravital imaging of CX3CR1⁺ KikRed⁺ cells in the spleen of Oil/CCl₄-treated mice after spleen photoconversion. The time-lapse intravital imaging was acquired by a 20×/0.75 NA objective. CX3CR1⁺ cells are shown in green, photoconverted CX3CR1⁺ cells are shown in red and the AF647 anti-CD31 labeled splenic vessels are shown in blue. Scale bar, 20 μm.

Movie S10: Intravital imaging of dynamic interaction between the splenic CX3CR1⁺ KikRed⁺ cells and hepatic CX3CR1⁺ KikGreen⁺ cells in the fibrotic liver at 24 h after photoconversion. The time-lapse intravital imaging was acquired by a 20×/0.75 NA objective. CX3CR1⁺ cells are shown in green, photoconverted splenic CX3CR1⁺ cells are shown in red. Scale bar, 50 μm.

Movie S11: Intravital imaging of stable interaction between the splenic CX3CR1⁺ KikRed⁺ cells and hepatic CX3CR1⁺ KikGreen⁺ cells in the fibrotic liver at 24 h after photoconversion. The time-lapse intravital imaging was acquired by a 20×/0.75 NA objective. CX3CR1⁺ cells are shown in green, photoconverted splenic CX3CR1⁺ cells are shown in red and the AF647 anti-CD31 labeled hepatic vessels are shown in blue. Scale bar, 50 μm.

Supplementary Table 1. Primer sequences.

mRNA	Forward (5′–3′)	Reverse (5′–3′)
α-SMA	GTCCCAGACATCAGGGAGTAA	TCGGATACTTCAGCGTCAGGA
iNOS	GGAGTGACGGCAAACATGACT	TCGATGCACAACCTGGGTGAAC
COL1A1	GCTCCTCTTAGGGGCCACT	CCACGTCTCACCATTGGGG
IL-1β	GAAATGCCACCTTTTGACAGTG	TGGATGCTCTCATCAGGACAG
TNF-α	CCTGTAGCCCACGTCGTAG	GGGAGTAGACAAGGTACAACCC
Actin	GTGACGTTGACATCCGTAAAGA	GCCGGACTCATCGTACTCC